AN FRFT BASED REAL-TIME ESTIMATION OF MOVING TARGET ACCELERATION METHOD FOR FMCW RADAR

Qingbo Wang

College of Computer Science and Technology, Nanjing University of Aeronautics and Astronautics, Nanjing, China

ABSTRACT

This paper considers the problem of real-time estimating the moving target acceleration in frequency modulated continuous wave (FMCW) radar. Based on the accelerated target FMCW radar echo signal model, after utilizing KeyStone transform to eliminate the effect of range migration on the signal parameters estimation. An improved fractional Fourier transform (FrFT) and optimized the best matching rotation angle search strategy is proposed to estimate the chirp rate of doppler dimension echo signal related to the target acceleration. Compared with the traditional FrFT, the approach in this paper has less computation and significantly reduced processing time while ensuring estimation accuracy. The proposed method is demonstrated with simulation and measurement data.

KEYWORDS

FMCW Radar, Acceleration Estimate, Range Migration, Fractional Fourier Transform, Linear Frequency Modulated, Chirp Rate

1. INTRODUCTION

Current-generation FMCW automotive radar can accurately measure the velocity of moving targets [1]. However, many targets with high acceleration exist in actual driving scenarios. The lack of acceleration information may cause the automated driving system to be unable to accurately predict the target state and make proper path planning and decisions, which leads to an increased probability of traffic accidents. Therefore it is necessary to implement real-time measurement of moving target acceleration in FMCW radar systems.

Suppose the moving target is accelerated. Its echo signal in the doppler dimension can be regarded as a linear frequency modulated (LFM) signal. The acceleration estimation of the target can be turned into an LFM signal parameter estimation problem [2]. In addition, the range migration will affect the doppler dimensional signal phase, resulting in the signal being divided into multiple parts in the time-frequency plane and affecting the parameter estimation of the signal. The KeyStone transform is needed to decouple the range and doppler dimension before range FFT.

The solutions of LFM signal parameter estimation can be divided into two categories: time-frequency representation (TFR) and frequency-chirp rate representation (FCR) [9]. Short Time Fourier Transform (STFT) [3] as a typical example of linear TFR is widely used because of its simple and convenient implementation. Wigner-Ville distribution (WVD) [4] as representative of quadratic class TFR has perfect time-frequency concentration when estimating the mono-

component signal parameter. However, WVD-based methods have cross-term problems when dealing with multi-component LFM signals. Although various methods have been proposed to reduce cross-term effects, such as Pseudo Wigner Distribution (PWD) [5], smoothed Pseudo Wigner Distribution (SPWD) [6]. These methods are realized at the expense of time-frequency resolution. In addition, TFR-based methods can not directly obtain the parameters estimation of the LFM signal. The line detection algorithms are additionally needed to get the signal chirp rate, such as the Radon-Wigner transform (RWT) [7], Wigner-Hough transform (WHT) [8]. This significantly increases the computational cost and limits the application in engineering. Lv's Distribution (LVD) [9] as the FCR class method proposed in recent years. It can directly obtain the chirp rate of the LFM signal without additional calculations. Compared to WVD, LVD can avoid interference by cross terms and is more easily implemented in engineering. However, the maximum chirp rate estimation of LVD is affected by the sampling rate, which causes the estimated acceleration to be ambiguous.

FrFT [10] as the generalization of the traditional Fourier transform, widely used in LFM signal detection and parameter estimation. FrFT converts the LFM signal from the time domain to the fractional Fourier domain by rotating the time-frequency plane. It has the best energy concentration in a specific fractional Fourier domain. Moreover, The discrete FrFT proposed by Ozaktas [11], Pei [12] makes FrFT can be implemented by FFT and chirp signal convolution. It is well suited for engineering applications.

This paper proposes a new algorithm for LFM signal chirp rate estimation based on the FrFT. It simplifies the traditional FrFT and has a more concise form. And based on the feature that the fractional domain spectrum of the improved FrFT is symmetric on both sides of the optimal rotation angle. An optimized search strategy is applied to avoid the global search of the rotation angle, which significantly reduces the processing time. After implementing the algorithm in a radar system, the actual environment tests proved that the algorithm could effectively and accurately estimate the acceleration of a moving target.

2. FMCW RADAR SIGNAL AND SYSTEM MODELS

In order to measure target range and velocity, the FMCW radar will transmit a series of LFM signals (or chirp pulses) with a total number of N through the transmitting antenna (Tx).
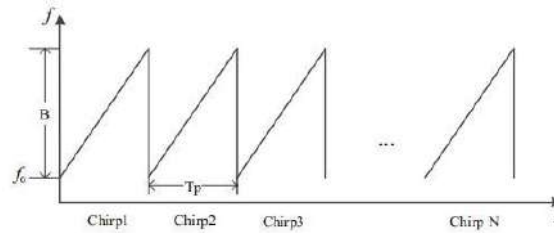

Figure 1. FMCW continuous transmit pulses time-frequency figure

As shown in Figure 1, the LFM signal with start frequency f_0 and its frequency increases linearly at rate of K over the time duration T_p [1].

2.1. IF Signal Model

The LFM signal transmitted by Tx can be expressed as:

$$S_t(t) = \exp[j(2\pi f_0 t + \pi K t^2)] \quad t \in (0, T_p) \tag{1}$$

When the transmitted signal strikes the target, it will reflect back and be received by the receiving antenna (Rx). The signal received by the Rx can be seen as a version of the transmitted signal after time delay τ. That is:

$$S_r(t) = \exp\{j[2\pi f_0(t-\tau) + \pi K(t-\tau)^2]\} \quad t \in (0, T_p) \tag{2}$$

When the radar system receives the signal reflected from the target, the echo signal is mixed with the transmitted signal through a mixer. The resulting signal is filtered low-pass to produce an intermediate frequency (IF) signal $S_I(t)$. The IF signal can be expressed as:

$$S_I(t) = S_t(t) \cdot S_r^*(t) = \exp\{j[2\pi(f_0\tau + K\tau t) - \pi K\tau^2]\} \quad t \in (0, T_p) \tag{3}$$

Assuming that there exists a moving target in front of the radar, the initial radial distance between radar and target is R_0. The target moves away from the radar with radial velocity v and constant radial acceleration a. Considering that the chirp pulse duration T_p is very short, the movement of the target within one chirp pulse is negligible. Only the movement between the two chirp pulses is considered. Therefore, the "Stop-and-Go" model is applied to establish for target echo signal. Based on the above assumption, one can get time delay of the nth chirp pulse:

$$\tau_n = \frac{2(R_0 + vnT_p + \frac{1}{2}an^2T_p^2)}{c} \quad n \in [0, N-1] \tag{4}$$

where c is the speed of light. Substituting τ_n into IF signal $S_I(t)$ and neglecting the τ^2 term in equation (3) (because $\tau^2 \approx c^{-2}$, its value is very small), the nth IF signal can be derived as follows:

$$S_I(t,n) = \exp\left\{j2\pi\left[\frac{2R_0f_0}{c} + \left(\frac{2R_0K}{c} + \frac{2KvnT_p}{c} + \frac{Kan^2T_p^2}{c}\right)t + \frac{2f_0v}{c}nT_p + \frac{f_0a}{c}n^2T_p^2\right]\right\} \tag{5}$$

$$t \in (0, T_p) \quad n \in [0, N-1]$$

To perform digital signal processing, the IF signal $S_I(t)$ is sampled with sampling frequency f_s and sampling period $T_c = 1/f_s$. Total M points are sampled. The sampled IF signal can be expressed as:

$$S_I(m,n) = \exp\left\{j2\pi\left[\frac{2R_0f_0}{c} + \left(\frac{2R_0K}{c} + \frac{2KvnT_p}{c} + \frac{Kan^2T_p^2}{c}\right)mT_c + \frac{2f_0v}{c}nT_p + \frac{f_0a}{c}n^2T_p^2\right]\right\} \tag{6}$$

$$m \in [0, M-1] \quad n \in [0, N-1]$$

After sampling the IF signal for all periods, we can get an $M*N$ two dimensional discrete time signal $S_I(m,n)$. One of the dimensions is fast time dimension (or range dimension) mT_c and the another is slow time dimension (or doppler dimension) nT_p. It is clear in equation (6), the frequency and phase of IF signal is:

$$f_{IF} = \frac{2R_0K}{c} + \frac{2KvnT_p}{c} + \frac{Kan^2T_p^2}{c} \tag{7}$$

$$\varphi_{IF} = 2\pi(\frac{2R_0f_0}{c} + \frac{2f_0v}{c}nT_p + \frac{f_0a}{c}n^2T_p^2) \tag{8}$$

In equation (7), due to the presence of $2KvnT_p$ and $Kan^2T_p^2$ terms, IF signal frequency is not a constant which is related to the chirp pulse period number n. So fast time and slow time coupled with each other. As a result, when the target is moving at high speed and acceleration, the central

of range spectrum envelope will be shifted significantly. This phenomenon leads to an additional phase error of the spectrum peak between the range cell shifts after the range FFT, affecting the estimation of the chirp rate along the doppler dimension signal.

2.2. Range Migration Analysis

Performing K points range FFT for discrete IF signal (6), one can get:

$$X(k,n) = \sum_{m=0}^{M-1} S_I(m,n)\exp(-j2\pi k \frac{m}{M} f_s T_c)$$
$$= \exp(j\varphi_{IF})P_M(\frac{k}{M} f_s - f_{IF})$$

(9)

where $P_M(\cdot)$ can be regarded as a discrete Fourier transform with a rectangular window of length M. The result is an asinc function, which is a discrete form of the continuous sinc function. The expression of $P_M(\cdot)$ is:

$$P_M(f) = \sum_{m=0}^{M-1} \exp(j2\pi f m T_c)$$
$$= \frac{\sin(\pi f M T_c)}{\sin(\pi f T_c)}\exp[-j\pi f(M-1)T_c]$$

(10)

Based on equations (9) and (10), one can get the peak phase φ_{peak} of the range spectrum:

$$\varphi_{peak} = \varphi_{IF} - \pi(\frac{k_{peak}}{M} f_s - f_{IF})(M-1)T_c$$

(11)

where k_{peak} denotes spectrum peak index. Furthermore, the IF signal doppler frequency f_d can be viewed as the result of the derivation of phase φ_{peak} with respect to slow time nT_p. If the peak index k_{peak} is not dependent on variable nT_p, the f_d can be derived as:

$$f_d = \frac{1}{2\pi}\frac{d\varphi_{peak}}{dnT_p}$$
$$= \left[\frac{2f_0 v}{c} + \frac{Kv(M-1)T_c}{c}\right] + \left[\frac{2f_0 a}{c} + \frac{Ka(M-1)T_c}{c}\right]nT_p$$

(12)

Obviously, under the above assumptions, f_d is a linear function of variable nT_p, and the chirp rate is related to the acceleration of the target. By using the LFM signal parameters estimation algorithm, one can get the target acceleration estimated. But in practice, this is not a common scenario, the change of k_{peak} must be taken into account.

Consider a single TX radar system example. The chirp pulse parameters are as follows: f_0 = 77GHz; f_s = 5000sps; T_p = 110us; K = 40MHz/us; N = 256. The target initial velocity and acceleration are set to 0m/s and 30m/s^2. Performing range FFT for all chirp pulse periods. The index of range spectrum peak for each period is shown in Figure 2(a). All peaks appear at 273 range cell. Figure 2(b) is the result of unwrapping phase for spectrum peaks. Without range cell shift, the peak phase is a quadratic function of chirp periods index n. Compared to Figure 2, Figure 3 shows the spectrum peak index and phase for target acceleration 300m/s^2. There exist three shifts in range cell. Furthermore, the phase also have shifts at the same position.
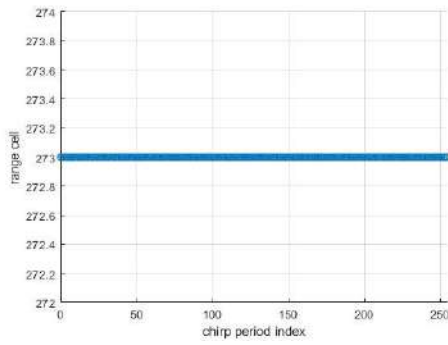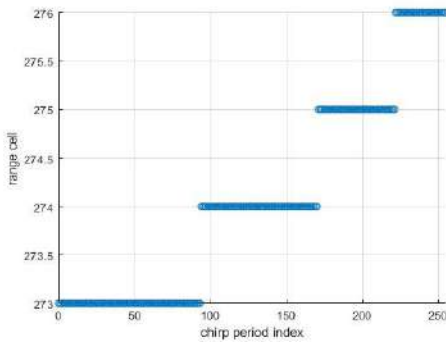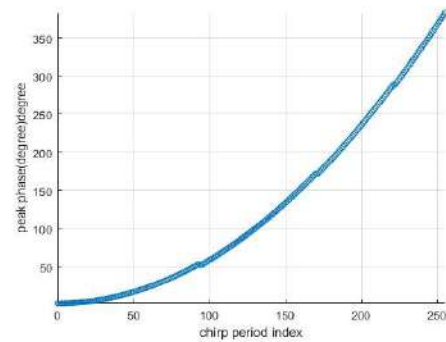
(a) peak index for all chirp periods
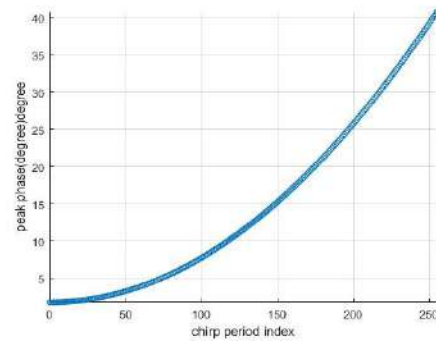
(b) peak phase without range cell shift

Figure 2. Range FFT results without range migration

(a) peak index for all chirp periods

(b) peak phase without range cell shift

Figure 3. Range FFT results with range migration

If we represent the peak phase of the above two cases in the time-frequency plane, the result is shown in Figure 4. When range cell shift is not present, the doppler signal is linearly distributed in the time-frequency plane as shown in Figure 4(a). Comparatively, when range cell is shifted, the doppler signal time-frequency distribution is divided into four segments, which is depicted in Figure 4(b). Ideally, the chirp rate of each segment is still the same. However, when there is noise in the signal, the chirp rate of each segment may vary greatly. In this case, the estimation error is much larger.
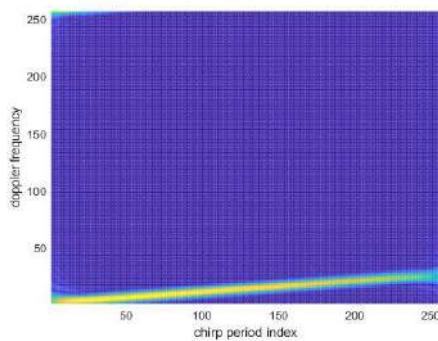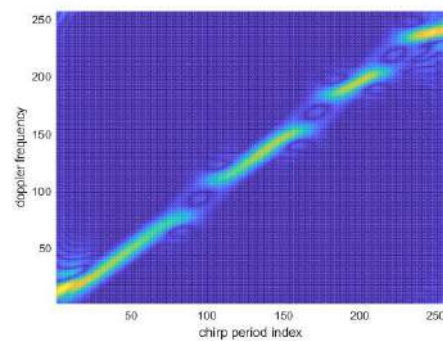
(a) peak index for all chirp periods   (b) peak phase with range cell shift

Figure 4. Doppler dimensional signal time-frequency distribution

2.3. KeyStone Transform

The KeyStone transform is well known in the field of synthetic aperture radar (SAR) for its capability of eliminating moving target range migration. According to the introduction in the previous section, the FMCW radar also has similar problems and affects the acceleration estimation of moving targets. Therefore, the KeyStone transform is applied before range FFT to decouple the fast and slow time. Based on the principle of KeyStone transform, putting the slow time terms in equation (6) together, one has:

$$S_I(m,n) = \exp\left\{ j\left[2\pi \frac{2R_0 f_0}{c} + 2\pi \frac{2R_0 K}{c} mT_c + 2\pi(f_0 + KmT_c)\frac{2vnT_p}{c} + 2\pi(f_0 + KmT_c)\frac{an^2 T_p^2}{c} \right] \right\} \quad (13)$$

Re-scale the slow time axis for each fast time sample point by follow transformation:

$$(f_0 + KmT_c)nT_p = f_0 n'T_p \quad (14)$$

Applying the scaling operator to (13), one can get:

$$S_I(m,n') = \exp\left\{ j\left[2\pi \frac{2R_0 f_0}{c} + 2\pi \frac{2R_0 K}{c} mT_c + 2\pi f_0 \frac{2vn'T_p}{c} + 2\pi f_0 \frac{an'^2 T_p^2}{c} \right] \right\} \quad (15)$$

Equation (15) indicates that for the new slow time $n'T_p$, the coupling between the slow time and fast time has been removed. By performing range FFT on (15), the central signal spectrum envelope will be located at $2R_0 K/c$, which is only related to the initial distance of the target R_0. That is, the range FFT for all chirp periods will peak at the same index. The range spectrum peak phase and doppler frequency can be re-expressed as:

$$\varphi'_{peak} = 2\pi\left[\frac{2R_0 f_0}{c} + \frac{2f_0 v}{c}nT_p + \frac{f_0 a}{c}n^2 T_p^2 - \left(\frac{k_{peak}}{M}f_s - \frac{2R_0 K}{c}\right)\frac{(M-1)T_c}{2}\right] \quad (16)$$

$$f'_d = \frac{1}{2\pi}\frac{\varphi'_{peak}}{dnT_p} = \frac{2f_0 v}{c} + \frac{2f_0 a}{c}nT_p \quad (17)$$

From the above equation, it can be seen that after KeyStone transform, without k_{peak} term influence, the doppler dimension signal changes to LFM signal that chirp rate only related to target acceleration.

The KeyStone transform can be implemented by the Chirp-Z transform and realization details can be referred to [13]. This paper will not discuss its implementation. In the following, we will analyze how to estimate the LFM signal chirp rate by improved FrFT.

3. THE LFM SIGNAL CHIRP RATE ESTIMATION VIA IMPROVED FRFT

3.1. Fractional Fourier Transform

Firstly, let us briefly reviews the definition of FrFT. Consider a mono-component LFM signal $f(t)$. For the convenience of derivation, the initial frequency of the $f(t)$ is set to 0.

$$f(t) = A\exp(j\pi Kt^2) \quad t \in (-T_d/2, T_d/2) \quad (18)$$

The formal FrFT of *f(t)* at an arbitrary rotation angle α is given by equation (19):

$$F^{\alpha}\left[f(t)\right]=X_{\alpha}(u)=\int_{-\infty}^{+\infty}f(t)K_{\alpha}(t,u)dt \tag{19}$$

where $K_{\alpha}(t,u)$ is the transform kernel and defined by (20):

$$K_{\alpha}(t,u)=\begin{cases}\sqrt{1-j\cot\alpha}e^{j(\pi u^2\cot\alpha-2\pi u c\csc\alpha+\pi^2\cot\alpha)}, & \alpha\neq k\pi \\ \delta(t-u), & \alpha=2k\pi \\ \delta(t+u), & \alpha=(2k+1)\pi\end{cases} \tag{20}$$

FrFT can be divided into the four steps:

(1) Perform de-chirp operation by modulate with a chirp $\exp(j\pi t^2\cot\alpha)$.
(2) Perform scale Fourier transform of the de-chirped signal by the scale factor $\csc\alpha$.
(3) Perform another modulate operation with chirp $\exp(j\pi u^2\cot\alpha)$.
(4) Multiply amplitude factor $\sqrt{1-j\cot\alpha}$.

The FrFT can be regarded as the process of signal projection on different chirp base functions. The energy intensity of signal in FrFT domain reflects the degree of similarity between the signal and chirp base functions. It will peak at the optimal rotation angle only when the parameters of the chirp base functions match the sought signal.

3.2. Improved Fractional Fourier Transform

Step 1 includes a chirp modulation, which makes FrFT adaptive to process the LFM signal. *Step 2* transforms the signal from the time domain to the FrFT domain. *Step 3* and *4* are performed to guarantee the FrFT additivity of rotation property and energy conservation property. The additivity property is important in some applications, but our purpose is to obtain the signal chirp rate. Whether *Step 3* is performed or not does not significantly affect the results. In consideration of saving hardware resources, we combine *Step 1*, *Step 2* and *4* to form an improved FrFT. The improved FrFT and its kernel can be expressed as:

$$\hat{F}^{p}\left[f(t)\right]=\hat{X}_{\alpha}(u)=\int_{-\infty}^{+\infty}f(t)\hat{K}_{\alpha}(t,u)dt \tag{21}$$

$$\hat{K}_{\alpha}(t,u)=\sqrt{1-j\cot\alpha}e^{j(\pi^2\cot\alpha-2\pi u c\csc\alpha)}\quad \alpha\in(0,\pi) \tag{22}$$

Since the improved FrFT no longer has the rotational additive property after omitting *Step 3*, we set the rotation angle scope from *0* to π. This is sufficient to cover the possible scope of the unknown parameters LFM signal chirp rate.

The improved FrFT is a special form of LCT. If we set a special parameter matrix $A=\begin{bmatrix}\cos\alpha & \sin\alpha \\ -\csc\alpha & 0\end{bmatrix}$, the LCT reduces to improved FrFT [14]. Using the properties of the LCT,

we can derive some important properties of improved FrFT, which are essential to the subsequent analysis.

(1) The time-shift property

$$\hat{F}^{p}\left[f(t-\tau)\right]=\hat{X}_{\alpha}(u-\tau\cos\alpha)e^{j(\pi\tau^2\cot\alpha-2\pi u c\csc\alpha)} \tag{23}$$

(2) The frequency-shift property

$$\hat{F}^{p}\left[f(t)e^{jvt}\right]=\hat{X}_{\alpha}(u-v\sin\alpha) \tag{24}$$

(3) The invertibility property

$$f(t) = \int_{-\infty}^{+\infty} \widehat{X}_\alpha(u)\widehat{K}_\alpha^*(u,t)du \tag{25}$$

(4)   The energy conservation property

$$\int_{-\infty}^{+\infty} |f(t)|^2 \, dt = \int_{-\infty}^{+\infty} |\widehat{X}_\alpha(u)|^2 \, dt \tag{26}$$

Similar to FrFT, the improved FrFT can also be expressed in terms of the WVD. The WVD of signal $f(t)$ is defined as:

$$WVD(t,\omega) = 2e^{j2\omega t}\int_{-\infty}^{+\infty} f(\tau)f^*(2t-\tau)e^{-j2\omega\tau}d\tau \tag{27}$$

Applying the time shift property to the $f^*(2t - \tau)$ term of the above equation:

$$WVD(t,\omega) = 2e^{j2\omega t}\int_{-\infty}^{+\infty}\widehat{X}_\alpha^*(-u+2t\cos\alpha)e^{-j(2t^2\cot\alpha-2tu\csc\alpha)}\int_{-\infty}^{+\infty}x(\tau)\widehat{K}_\alpha(\tau,u)e^{-j2\omega\tau}d\tau du \tag{28}$$

Then use frequency-shift property to compute inner integral in equation (28) and make the change of variable $\varepsilon = u + 2\omega\sin\alpha$, it comes to:

$$WVD(t,\omega) = 2\int_{-\infty}^{+\infty}\widehat{X}_\alpha(\varepsilon)\widehat{X}_\alpha^*(-\varepsilon+2t\cos\alpha+2\omega\sin\alpha)e^{-j(2t^2\cot\alpha-2t\varepsilon\csc\alpha+4\omega t)}d\varepsilon \tag{29}$$

Finally, making following change of variables from (t,ω) to (u,v):

$$u = t\cos\alpha + f\sin\alpha$$
$$v = -t\csc\alpha \tag{30}$$

The final result can be obtained as:

$$WVD(t,\omega) = 2e^{j2uv}\int_{-\infty}^{+\infty}\widehat{X}_\alpha(\varepsilon)\widehat{X}_\alpha^*(2u-\varepsilon)e^{-j2v\varepsilon}d\varepsilon \tag{31}$$

From the perspective of axis rotation, the improved FrFT of signal can still be seen as the result of rotating the t - f axis to the u - v axis. Compared to the traditional FrFT, the difference is only reflected in the position of the v-axis. The rotation of the signal from the time t-axis to the u-axis is entirely the same. That is say, after performing improved FrFT, the spectral support interval of the signal in u-axis is the same as traditional FrFT. It can be represented in Figure 5.
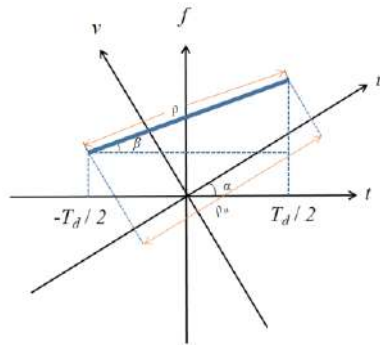

Figure 5. Representation of LFM signal in the t-f and u-v plane

The blue line in Figure 5 is the distribution line of the signal in the time-frequency plane, whose angle with the time axis t is β. The width of the signal in the time-frequency plane can be expressed as:

$$\rho = \frac{T_d}{|\cos\beta|} \tag{32}$$

Considering the improved FrFT with rotation angle α. ρ_u in Figure 5 is the projection length of the LFM signal in the u-axis after the transformation. According to the geometric relationship in Figure 5, the expression of ρ_u can be obtained as:

$$\rho_u = \left| \frac{T_d \cos(|\alpha - \beta|)}{\cos\beta} \right| \tag{33}$$

Since the angle between signal and the time axis is fixed, the magnitude of ρ_u is related to the rotation angle α. When $\alpha = \beta + \pi/2$, the width of the support interval becomes a dot where the energy of the signal is concentrated. Otherwise, the energy is divided equally by the support interval, which approximates a rectangle inside the support interval, and outside the rectangle, the energy of the signal drops sharply. The expressions for the energy magnitude in the support interval are derived following by definition of improved FrFT.

When the rotation angle α is the finite length LFM signal $f(t)$ optimal rotation angle, i.e. α = -arccot(-K). Equation (21) can be turned into:

$$\widehat{X}_\alpha(u) = A\sqrt{1 - j\cot\alpha} \int_{-T_d/2}^{T_d/2} e^{j[\pi(K+\cot\alpha)t^2 - 2\pi u \csc\alpha]} dt$$
$$= A\sqrt{1 - j\cot\alpha} T_d \sin c(\pi T_d u \csc\alpha) \tag{34}$$

From the equation (34), it can be seen that the transformation of the signal at the optimal rotation angle results in a sinc function. The peak is located at $u = f_0 \csc\alpha$.

When $\alpha \neq$ -arccot(-K), after some derivations of equation (21), one can get:

$$\widehat{X}_\alpha(u) = A\sqrt{\frac{1 - j\cot\alpha}{2(K+\cot\alpha)}}\sqrt{[c(T_1) + c(T_2)]^2 + [s(T_1) + s(T_2)]^2} e^{j\left[\arctan\frac{s(T_1)+s(T_2)}{c(T_1)+c(T_2)} - \pi\frac{(u\csc\alpha)^2}{K+\cot\alpha}\right]} \tag{35}$$

where $c(T)$ and $s(T)$ can be expressed as:

$$c(T) = \int_0^T \cos\left(\frac{\pi}{2}z^2\right)dz$$
$$s(T) = \int_0^T \sin\left(\frac{\pi}{2}z^2\right)dz \tag{36}$$

T_1 and T_2 can be expressed as:

$$T_2 = \sqrt{2(K+\cot\alpha)}\left(\frac{T_d}{2} - \frac{u\csc\alpha}{K+\cot\alpha}\right)$$
$$-T_1 = \sqrt{2(K+\cot\alpha)}\left(-\frac{T_d}{2} - \frac{u\csc\alpha}{K+\cot\alpha}\right) \tag{37}$$

Compared with conventional FrFT, the spectral amplitude of the signal in the improved FrFT support interval is equal to FrFT. The difference between them is only in the phase term. But this will not affect our aim to search for the optimal rotation angle. The spectral amplitude of signal can be expressed as:

$$\left|\widehat{X}_\alpha(u)\right| = A\sqrt{\frac{1 - j\cot\alpha}{2(K+\cot\alpha)}}\sqrt{[c(T_1) + c(T_2)]^2 + [s(T_1) + s(T_2)]^2} \tag{38}$$

Consider the case where the spectrum amplitude is the maximum. Due to the assumption that the initial frequency of the signal is 0 in the above, it will peak at 0 in u-axis. Substituting $u = 0$ into the equation (38) and assume that $T_d\sqrt{K+\cot\alpha} >> 1$. The Fresnel integral in equation (38) have $c(T) = s(T) \approx 0.5$. Then we can obtain the maximum spectral amplitude expression:

$$\left|\hat{X}_\alpha(0)\right| = A\sqrt{\frac{1-j\cot\alpha}{2(K+\cot\alpha)}} \tag{39}$$

When the spectral support interval is $[-\rho_u/2, \rho_u/2]$, taking $u = \pm\rho_u/2$ into equation (38), one can get:

$$\left|\hat{X}_\alpha(\pm\frac{\rho_u}{2})\right| = \frac{A}{2}\sqrt{\frac{1-j\cot\alpha}{2(K+\cot\alpha)}} \tag{40}$$

From equation (40), we can obtain that when the support interval is ρ_u, the amplitude becomes half of the maximum value. Furthermore, the value of the Fresnel integral function fluctuatingly decreases with the increase of $T_d\sqrt{K+\cot\alpha}$. The shape of the spectrum is closer to a rectangle, and energy of the signal is mainly concentrated in the support interval. While outside the support interval, the amplitude of the signal spectrum is very small [15].

We have derived the spectral characteristics of the continuous signal above. But in practice, we are dealing with discrete signals. So it is necessary to consider the spectral characteristics of the discrete signals. The discrete improved FrFT can be implemented using the FFT-based algorithm proposed by Ozaktas [11]. This algorithm needs to normalize the dimensional before calculation. Since the time and frequency domain have different magnitudes. For the convenience of calculation, both of them are converted into a normalized domain. Define the normalization factor $S = \sqrt{T_d/f_s}$, the signal time domain interval $[-T_d/2, T_d/2]$ and frequency domain interval $[-f_s/2, f_s/2]$ is converted to $[-\Delta x/2, \Delta x/2]$, where $\Delta x = \sqrt{T_d f_s}$. In normalized dimensional the sample interval changes to $1/\Delta x$ and the number of samples is N, where $N = \Delta x^2$.

Based on the assumptions of method II in [11]. To satisfy the sampling theorem, the signal needs to be twice interpolated. After interpolating the signal using sinc interpolation algorithm and some algebraic manipulations similar in [11]. The discrete improved FrFT can be written as:

$$\hat{X}_\alpha(\frac{m}{2\Delta x}) = \frac{\sqrt{1-j\cot\alpha}}{2\Delta x} e^{-j\pi\csc\alpha(\frac{m}{2\Delta x})^2} \sum_{n=-N}^{N} e^{j\pi\csc\alpha(\frac{m-n}{2\Delta x})^2} e^{j\pi(\cot\alpha-\csc\alpha)(\frac{n}{2\Delta x})^2} f(\frac{n}{2\Delta x}) \tag{41}$$

where m is the discrete sampling point of FrFT domain, $m \in [-M, M]$. It can be recognized that equation (41) is the result of convolving the signal $f(t)$ with $\exp(j\pi t^2\cot\alpha)$ after modulated by $\exp[j\pi t^2(\cot\alpha-\csc\alpha)]$. The improved FrFT requires only one signal twice interpolation and extraction, one chirp signal multiplication and one signal convolution operation.

Replace $f(n/2\Delta x) = A\exp[j\pi K(n/2\Delta x)^2]$ in equation (41) and set $K = -\cot\alpha_0$:

$$\hat{X}_{\alpha_0}(\frac{m}{2\Delta x}) = \frac{A\sqrt{1-j\cot\alpha_0}}{2\Delta x} \sum_{n=-N}^{N} e^{-j\pi\csc\alpha_0\frac{2mn}{(2\Delta x)^2}} \tag{42}$$

When $m = 0$ in equation (42), we can obtain the maximum amplitude of the discrete signal spectrum:

$$\left|\widehat{X}_{\alpha_0}(0)\right| = \frac{|A|\,|\sqrt{1-j\cot\alpha_0}|\,(2N+1)}{2\Delta x} \approx \frac{|A|\,\sqrt{N}}{\sqrt{\sin\alpha_0}} \qquad (43)$$

Denote the energy of the signal $f(t)$ by E and applying the energy conservation property (26):

$$E = \left|\widehat{X}_{\alpha_0}(0)\right|^2 = \frac{AN}{\sin\alpha_0} \qquad (44)$$

where α_0 is the optimal rotation angle and have $\alpha_0 = \beta + \pi/2$. After normalization, the geometric relationship in Figure 5 changes to:

$$\cos\beta = \frac{\Delta x}{\sqrt{(KT_dS)^2 + (\Delta x)^2}} \qquad (45)$$

$$\rho = \frac{\Delta x}{\cos\beta} = \sqrt{T_d f_s + \frac{K^2 T_d^3}{f_s}} \qquad (46)$$

$$\rho_u = \left|\rho\cos(\frac{\pi}{2} + |\alpha - \beta|)\right| = \rho\sin(|\alpha - \beta|) \qquad (47)$$

In the normalized domain, the sample interval is $1/\Delta x$. And we can get the number of sampling points M of the signal in support interval $M = \rho_u\Delta x$. In the support interval, the signal energy can be approximated as being equally divided by the sampling points M. Hence we can obtain the following:

$$E = \left|\widehat{X}_\alpha(m)\right|^2 M \qquad (48)$$

Combining equation (44) with equation (48), one has:

$$\left|\widehat{X}_\alpha(m)\right| = \frac{A}{\sqrt{\sin|\alpha - \alpha_0|}} \qquad (49)$$

3.3. Optimal Rotation Angle Search Strategy

Similarly to FrFT, the improved FrFT also need to scan for all rotation angles and search for peaks in the formed α-u plane. However, this kind of method has two shortcomings. On the one hand, when the parameter estimation accuracy is high, it needs to set a smaller search step size, which leads to a very time-consuming calculation of improved FrFT and peak search in the two-dimensional plane. On the other hand, storing this data in the radar hardware system is very memory consuming. In order to avoid performing improved FrFT for each value of α, we employ an improved search strategy to reduce the computational cost while ensuring the accuracy of signal parameter estimation.

From equation (49), the spectral amplitude of the signal in the FrFT domain is symmetric on both sides of the optimal rotation angle. We can simplify the process using this feature by applying a two-level search. First, perform the improved FrFT with a larger step size. Search the location of the peak and compare the peak with the difference in amplitude between the left and right sides. According to the symmetry property, the optimal rotation angle will appear on the side with a smaller values of difference. Then perform the improved FrFT on this side with smaller step size. Repeat the above steps until the expected accuracy.

4. SIMULATION

Example 1: The process of estimating the LFM signal chirp rate of the improved FrFT algorithm is shown in this example. Consider an LFM signal $\exp(j\pi2000t^2)$ which is sampled with

parameters f_s = 4000Hz, T_d = 1s. Set the step size of coarse search to 0.01, and the result is shown in Figure 6(a). It is clear from the figure that order 1.3 is the optimal order. Comparing the difference between the 1.3 order and its left and right side orders. We can determine that the optimal rotation order is in (1.29, 1.30). In this scope continue performing the improved FrFT with a smaller step size of 0.001. The results are shown in Figure 6(b).

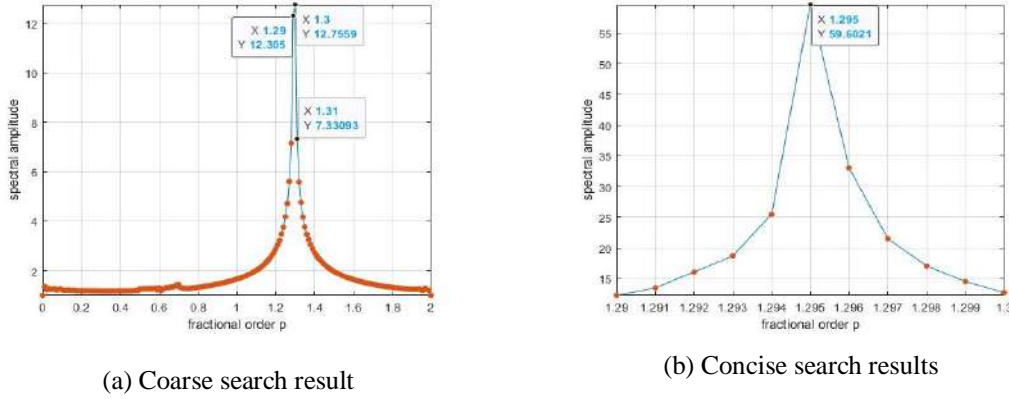| (a) Coarse search result | (b) Concise search results |

Figure 6. The improved FrFT two-level search

The maximum amplitude order in the Figure 6(b) is 1.295. From the relationship between the rotation order p and the chirp rate of the signal $K = -\cot(p\pi/2)f_s/T_d$. We can get the estimation of the chirp rate is 1998.7Hz/s. The estimation error is 1.3Hz/s.

Example 2: To evaluate the improved FrFT performance, we add Gaussian white noise to the signal in *Example 1*. The signal to noise ratio (SNR) varies from −10 to 5dB. For each SNR value, total 1000 trials are performed. Figure 7 shows that the improved FrFT and search strategy still has good estimation performance at -6dB noise condition.
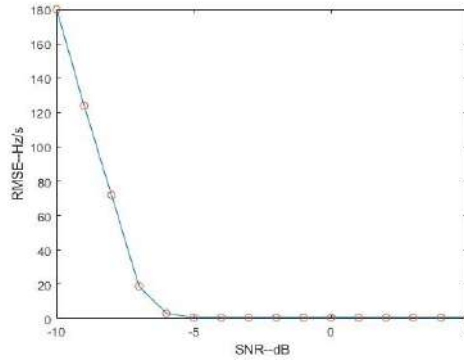

Figure 7. RMSE versus SNR for the chip rate

Example 3: This example is to demonstrate the efficiency of the improved algorithm. The same signal from *Example 1* is used and adds -5dB noise. Compare the improved FrFT algorithm with the conventional FrFT of 0.01, 0.001 and 0.0001 step sizes. The estimated errors and processing times are shown in the Table 1. Simulation results indicate that the improved FrFT can achieve the accuracy of traditional FrFT in 0.0001 step size, and the processing time is 1/3500 of the original.

Table 1. Comparison of the efficiency between improved algorithm and traditional FrFT

| Algorithm	Step Size	Estimated Chirp Rate (Hz/s)	Estimated Error (Hz/s)	Running Time (s)
Conventional FrFT	0.01	2038.6	38.6	0.82
Conventional FrFT	0.001	1991.3	8.7	10.68
Conventional FrFT	0.0001	1998.7	1.3	138.52
Improved FrFT	-	2001.5	1.5	0.04

5. EXPERIMENTAL RESULTS

In order to demonstrate the effectiveness of the proposed algorithm in real scenarios. We implemented the algorithm in the TI 2243p cascade radar system and tested it in a reality situation. The test environment is shown in Figure 8.
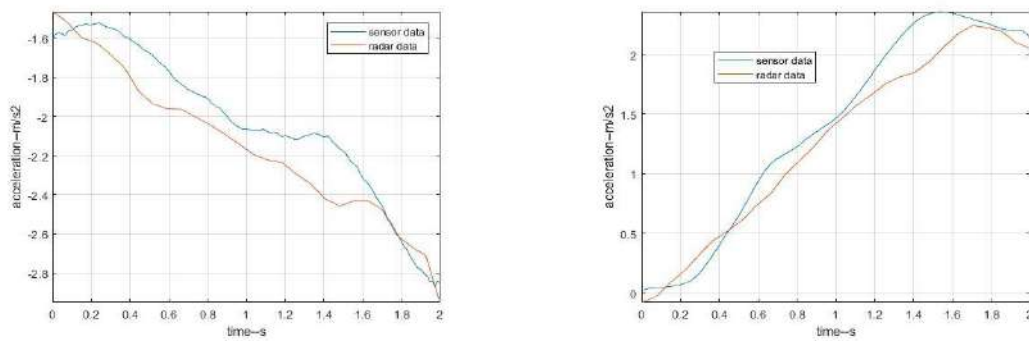

Figure 8. Acceleration measurement experiment scenario

In the experiment, a car was located in front of the radar. After the experiment started, driving the car made acceleration and deceleration motions while turning on the radar to collect the data. In order to verify the accuracy of the radar data, we placed an acceleration sensor on the car for data comparison while the car was driving. After saving the radar and sensor data, the acceleration change curve of both is drawn by Matlab. The result is shown in Figure 9.
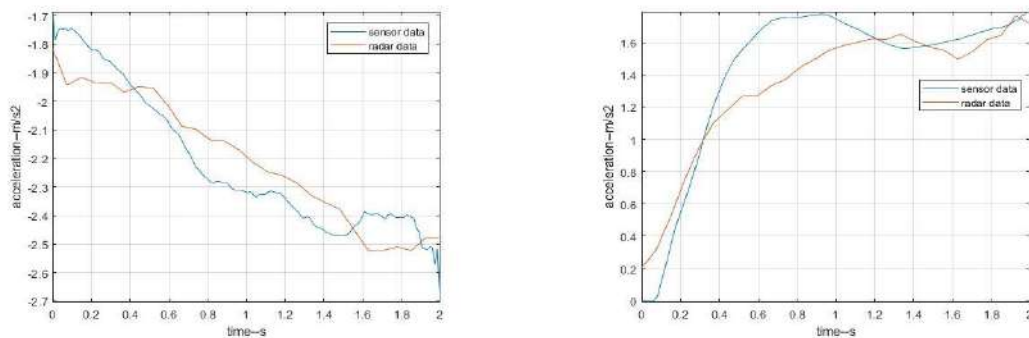
(a) The first set of experimental measurements

(b) The second set of experimental measurements

Figure 9. Actual scenario car acceleration measurement results

The experimental results prove that this paper's algorithm can effectively measure a moving target's acceleration. The estimation accuracy can reach $0.2m/s^2$. In addition, the improved FrFT can greatly reduce the data processing time. The processing time of one frame is about 50us, which meets the real-time requirement of the radar system.

6. CONCLUSIONS

This paper proposes a method to measure the acceleration of moving targets for FMCW radar. This method first addresses the problem of range migration in FMCW radar system. Then a more concise and efficient improved FrFT is performed to obtain the chirp rate of the signal and accordingly get the acceleration estimate. Simulation with Matlab and actual scenario tests are presented to validate the proposed method.

ACKNOWLEDGEMENTS

REFERENCES

[1]   Li, X & Wang, X & Yang, Q & Fu, S, (2021) "Signal processing for TDM MIMO FMCW millimeter-wave radar sensors", IEEE Access, Vol. 9, pp167959-167971.
[2]   Hassanien, A & Vorobyov, S. A & Gershman, A. B, (2012) "Moving target parameters estimation in noncoherent MIMO radar systems", IEEE Transactions on Signal Processing, Vol. 60, No. 5, pp2354-2361.
[3]   Portnoff, M. (1980) "Time-frequency representation of digital signals and systems based on short-time Fourier analysis", IEEE Transactions on Acoustics, Speech, and Signal Processing, Vol. 28, No. 1, pp55-69.
[4]   Claasen, T. & Mecklenbraeuker, W. (1980) "The wigner distribution - a tool for time-frequency signal analysis. i: continuous-time signals", Philips Journal of Research, Vol. 35, No. 14.
[5]   Gonalves, P. & Baraniuk, R. G. (1998) "Pseudo affine wigner distributions : definition and kernel formulation", IEEE Transactions on Signal Processing, Vol. 46, No. 6, pp1505-1516.
[6]   Stankovic, L. (1994) "A method for time-frequency analysis", Signal Processing IEEE Transactions on, Vol. 42, No. 1, pp225-229.
[7]   Wood, J. C. & Barry, D. T. (1992) "Radon transformation of time-frequency distributions for analysis of multicomponent signals" Signal Processing IEEE Transactions on, Vol. 42, No. 11, pp3166-3177.
[8]   Barbarossa, S. (1995) "Analysis of multicomponent lfm signals by a combined wigner-hough transform", IEEE Transactions on Signal Processing, Vol. 43, No. 6, pp1511-1515.

[9]   Lv, X & Bi, G & Wan, C & Xing, M. (2011) "Lv's distribution: principle, implementation, properties, and performance", IEEE Transactions on Signal Processing, Vol. 59, No. 8, pp3576-3591.

[10] Almeida, L. B. (1994) "The fractional Fourier transform and time-frequency representations", IEEE Transactions on signal processing, Vol. 42, No. 11, pp3084-3091.

[11] Ozaktas, H. M. & Arikan, O. & Kutay, M. A. & Bozdagt, G. (1996) "Digital computation of the fractional Fourier transform". IEEE Transactions on signal processing, Vol. 44, No. 9, pp2141-2150.

[12] Pei, S. C. & Ding, J. J. (2000) "Closed-form discrete fractional and affine Fourier transforms", IEEE transactions on signal processing, Vol. 48, No. 5, pp1338-1353.

[13] Richards, M. A. (2014) "The keystone transformation for correcting range migration in range-doppler processing", pulse, 1000, 1.

[14] Guo, Y & Yang, L (2019) "Method for parameter estimation of LFM signal and its application", IET Signal Processing, Vol. 13, No. 5, pp538-543.

[15] Xu, H. F & Liu, F. (2010) "Spectrum characteristic analysis of linear frequency-modulated signal in the fractional Fourier domain", Signal Process, Vol. 26, No. 12, pp1896-1901.

AUTHORS

Qingbo Wang was born in Jiangxi, China, in 1997. He is currently pursuing the Master's degree in Nanjing University of Aeronautics and Astronautics, Nanjing, China. Currently, the major research focus is on signal processing for mmWave radar.